ELSEVIER

Biophysical Chemistry 51 (1994) 21–35

Biophysical Chemistry

Glycolytic pH oscillations in a flow reactor ☆

Craig G. Hocker [a,1], Irving R. Epstein [a], Kenneth Kustin [a,*], Keith Tornheim [b]

[a] *Department of Chemistry, Brandeis University, P.O. Box 9110, Waltham, MA 02254-9110 (USA)*
[b] *Department of Biochemistry and Diabetes and Metabolism Unit, Boston University School of Medicine, Boston, MA 02118 (USA)*

(Received 10 November 1993; accepted in revised form 17 December 1993)

Abstract

A new type of flow reactor (UCSTR) has been developed that uses anisotropic ultrafiltration membranes in a continuous flow stirred tank reactor (CSTR) to facilitate the study of nonlinear enzyme catalyzed reactions. The design allows the study of enzymes with subunit molecular weights $\geqslant 9000$ dalton and protein concentrations up to at least 2 mg/ml under flow conditions with a residence time of 3 min or more, in a reactor of volume 1.67 ml. The UCSTR allows continuous potentiometric or spectrophotometric measurement without design change. Calibration of reactor performance was carried out by reproducing pH oscillations in the ferrocyanide–hydrogen peroxide reaction. Experimental verification of oscillatory glycolysis in the UCSTR was carried out with extract of rat skeletal muscle. Input feeds were fructose-6-phosphate and ATP with low concentrations of phosphate as buffer. Oscillations in pH, sustained for over eight hours, were observed. A six-step mechanism, including product activation and substrate inhibition, seven concentration variables, and four enzymes sufficed to simulate the pH oscillations observed in the UCSTR.

Key words: Glycolysis; Oscillations; Ultrafiltering continuous flow stirred tank reactor

1. Introduction

The study of nonlinear chemical dynamics has been greatly facilitated by the use of reactors open to the exchange of matter with their surroundings [1]. Because of problems associated with enzyme loss in a conventional continuous flow stirred tank reactor (CSTR), the application of such reactors to biochemical reaction systems has been much more difficult to achieve. Alternative arrangements that minimize enzyme loss, including semi-batch reactors [2], chemical immobilization of enzymes [3,4], and enzyme entrapment, have been used with moderate success.

Enzyme entrapment within a polyacrylamide gel [5] suffers from the problem of enzyme leakage, which should be improved by entrapment within a sol-gel glass [6], since the inorganic ma-

* Corresponding author.

☆ Part 79 in the series Systematic Design of Chemical Oscillators. Part 78 is: I.R. Epstein, K. Kustin and R.H. Simoyi, J. Phys. Chem., 96 (1992) 5852.

[1] Present address: National Science Foundation Center for Biological Timing, Department of Biology, University of Virginia, Charlottesville, VA 22903-2477, USA.

Elsevier Science B.V.
SSDI 0301-4622(94)00025-F

trix should prevent leakage of the enzyme from the trap. However, such an approach introduces many unknown environmental factors into an already complicated system, which tends to obscure rather than clarify the system's reaction dynamics. Physical entrapment, which does not interfere with enzyme chemistry, should therefore be a better approach to enzyme containment than chemical entrapment.

Dialysis of proteins depends on a symmetric ultrafiltration membrane (SUM), which allows only small molecules to pass through it. A reactor incorporating a compartment containing an enzyme trapped behind such a membrane with selective diffusivity has been used to study sinusoidal (5 h) oscillations of phosphofructokinase catalysis [7].

A more sophisticated filter technology employs the composite asymmetric ultrafiltration membrane [8] (ASUM). A very thin (0.1–1.5 μm) polymer film is joined to one side of a much thicker (50–250 μm) porous structure made of the same material. Variation of pore diameter in the thin film permits different macromolecules to be selected for passage through the membrane. The thicker substrate enables the thinner film to withstand high flow rates. Clogging of the thinner membrane's pores is minimized, because the trapped macromolecule is rejected at the membrane surface. This type of membrane can be used to construct a reactor for the study of enzyme catalysis in flow. We describe such a reactor and its application to the detection and study of glycolytic pH oscillations.

2. Materials and methods

The glycolytic reaction step between α-D-fructose 6-phosphate (F6P) and adenosine 5′-triphosphate (ATP), which is catalyzed by rabbit skeletal muscle enzyme 6-phosphofructokinase (PFK) in the presence of magnesium(II) ions, is followed by monitoring the proton that is liberated in reaction (R1),

$$F6P^{2-} + MgATP^{2-} \xrightarrow{PFK} FDP^{4-} + MgADP^{-} + H^{+}, \qquad (R1)$$

where FDP is D-fructose 1,6-diphosphate and ADP is adenosine 5′-diphosphate.

This reaction is used as an index of progress at near neutral pH in the glycolytic sequence beginning with F6P and ending with lactate (LAC). All experiments were done at 25°C with a YM-30 ASUM for purified PFK and at 30°C with a YM-10 ASUM for extracts. In this section we present the materials and data collection methods used in this study. The design and construction details of the reactor are presented in the following section.

2.1. Materials and assays

For testing the reactor, reagent grade H_2O_2 (30%) and sulfuric acid (98%) (Fisher), and $K_4[Fe(CN)_6] \cdot 3H_2O$ (Sigma) were used without further purification.

Purified rabbit muscle PFK used in trial and preliminary experiments was obtained from Boehringer-Mannheim in a 3.2 M $(NH_4)_2SO_4$ suspension containing 10 mg/ml of protein, 10 mM potassium phosphate and 1 mM adenosine phosphate at pH 7.5. Boehringer–Mannheim's method of purifying PFK is based on an improvement [9] of an earlier commonly used method [10]. All suspensions were stored at 4°C. Bovine serum albumin (BSA) (Sigma) was a fatty acid-free (< 0.005%) powder stored desiccated at 4°C (99% albumin, remainder mostly globulins, Sigma A-6003).

For measuring PFK activity in batch, $(NH_4)_2SO_4$-free enzyme solutions were prepared by adding 0.050 ml of the $(NH_4)_2SO_4$ suspension of PFK to 2 ml of the desired solution in a Centricon-30 microconcentrator (Amicon) and centrifuging at $2000 \times g$ for 25 min. The final solution of about 0.050 ml was then diluted with 2 ml of solution (100 mM bis(2-hydroxyethyl)iminotris(hydroxymethyl)methane (Bis-Tris), 100 mM KCl, 50 mM NaCl, 3 mM $MgSO_4$, 1 mM K_2HPO_4) and centrifuged as before. This procedure was repeated 3 times. The remaining solution (about 0.025 ml) was diluted to the desired volume, and the microconcentrator was then inverted and centrifuged for 2 min at $500g$. The enzyme solution was stored in the retentate cup

at 4°C and used within 48 h. The standard assay of PFK was performed using a Varian DMS-200 spectrophotometer to monitor the absorbance of NADH at 340 nm produced by coupling enzymes which consumed the ADP produced by (R1). The coupling enzymes were a solution of pyruvate kinase (PK) and lactate dehydrogenase from rabbit muscle in 50% glycerol containing 10 mM 4-(2-hydroxyethyl)-1-piperazine ethanesulfonic acid (HEPES), 100 mM KCl, and 0.1 mM ethylenediaminetetraacetic acid (EDTA) at pH 7.0 (Sigma P-0294).

Solutions for flow experiments were prepared by first mixing separate concentrated salt/buffer, ATP, F6P, and 1,4-dithiothreitol (DTT)/β-nicotinamide adenine dinucleotide (NAD) solutions to a volume of 240 ml using as diluent deionized, neutral water containing 1.0 mM EDTA. The NAD (Sigma, 5 mg pre-weighed vials) and DTT were usually prepared within one day of the experiments, while the other solutions were prepared within one week. The mixture was stirred in a flask and adjusted to the correct pH using HCl with the same measuring equipment to be used in the experiment. The solution was transferred to a 250.0 ml volumetric flask, where it was diluted to the final volume with the EDTA solution. The solution was then poured into a Corning Disposable Sterile Filter assembly with a 0.22 μm cellulose acetate membrane. The filter cap unit was replaced with a custom cap seal after introducing a clean teflon stirrer into the storage bottle. The solution was then degassed by stirring for 10 min under aspirator vacuum (0.7 Torr), and stored at 4°C in a filter storage bottle until used. Nonreactant species unless otherwise mentioned are: 0.1 M KCl, 0.05 M NaCl, 6 mM $MgSO_4$, 1 mM EDTA, 0.1 mM DTT, 1 mM Bis-Tris, and 1 mM K_2HPO_4. Aspartate and guanosine-5'-triphosphate (GTP) were added to the DTT/NAD solution to prevent the irreversible loss of AMP due to the adenylate deaminase activity present in the extract by regenerating AMP through the purine nucleotide cycle [11].

For those experiments where yeast hexokinase (HK, Sigma) was added, HK was made $(NH_4)_2SO_4$-free as described above, and stored at 4°C in a solution containing 47 mM KCl, 7.5 mM phosphate, 8.33 mM $MgCl_2$, 1 mM EDTA, 0.1 mM DTT at pH 7.0. HK was assayed within a day of the experiment, and was stable for at least 2 weeks.

The final flow experiments utilized 2 ml frozen fractions of the gel-filtered, high-speed supernatant of rat hindleg muscle [12] stored at −70°C. The melted fraction was stored at 4°C and used within 48 h. A freshly melted extract was centrifuged at 4000 rpm for 5 min if significant precipitate was present. Quickly refreezing unused portions of extracts by immersion in liquid N_2 was not successful: protein precipitated and the supernatant had low activity. The extracts remained precipitate-free for a week when stored at 4°C under argon. Undiluted extract had a pH of 6.5 and contained 280 mM KCl, 15 mM phosphate, 5 mM EDTA, 0.1 mM DTT, and approximately 8 mg/ml protein.

2.2. Methods of data collection

Kinetics curves were obtained with either of two methods. For electrochemical measurements, the voltage signal was processed by a 12 bit analog/digital converter (Metrabyte DAS-8) (±5.0 V) and an 8088 PC (Coherent Technology) with 640 K RAM. Simultaneous measurement of the voltage signal from the chemical species detector (electrode) and the flow rate detector (photocell) was carried out by using custom programs written by one of us (CGH) [13] and the Quarterdeck Desqview multitasking environment for DOS (version 3.3). The voltage signal from the pH electrode was amplified by a custom-made gain 0–101, low pass filter (12 Hz), offset (±2.5 V) circuit. For optical absorbance measurements of adenine nucleotide concentration ($A_{262nm} - A_{282nm}$) or [NADH] (A_{340nm}), the optical signal and elapsed time data were acquired through an IBM PC integrated into a diode array spectrophotometer (Hewlett-Packard 8452A).

3. The UCSTR

The new flow reactor to be described is designed to provide continuous monitoring of enzy-

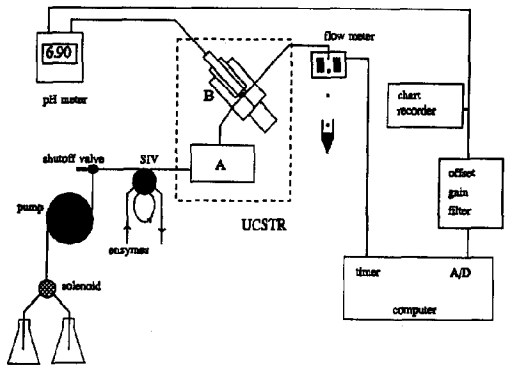

Fig. 1. Schematic diagram of UCSTR. The solenoid allows switching back and forth between input solutions. The shutoff valve relieves pressure of arrested pump when solutions are changed. The enzymes are injected into a 0.25 ml or 0.5 ml Teflon loop at the sample injection valve (SIV) which is used to insert enzyme solution into the reactor (A). (Detail for (A) in Fig. 2.) The input feed is split in two, entering the reactor at two inlets 180° apart. The stirrer rotates at 500 rpm using a double U-magnet. The outflow from the reactor (A) moves through a 0.15 ml stirred detection chamber (B) with a flat pH electrode. From B, the outflow travels through a 1/32 inch inner diameter teflon tube to a precision-cut leveled hole, where drops interrupt the infrared beam of the photocell used to monitor the flow rate.

matically catalyzed reactions. It incorporates an ASUM, and has been named the ultrafiltering continuous flow stirred tank reactor (UCSTR). In addition to the reactor–detector unit, other components required for a complete flow-through system (Fig. 1) are located in a reagent-handling pump unit and a data acquisition unit.

3.1. Pump unit

The pump unit consists of separate nonenzymatic degassed solution reservoirs at ambient temperatures and pressures, a pump, shutoff valve, and sample injection valve (SIV). In a continuously fed and stirred reactor, constant flow rate is essential to prevent the occurrence of artifactual oscillations. In the UCSTR, the ASUM offers much greater resistance to fluid flow than is encountered in conventional reactors. The Rainin Rabbit-plus peristaltic pump produced the smoothest and most constant flow of the pumps tested: flow rate fluctuations $< \pm 1\%$ in the flow range up to 30 ml h^{-1}. Small diameter (i.d. 0.25–0.50 mm) thick-walled silicone tubing is used in the pump. The tubing becomes deformed with use and is frequently replaced. The pump tubing is connected to the Teflon 1/16 inch delivery tubing by inserting a syringe needle with male Luer connector into the pump tubing and wrapping copper wire tightly around the tubing with pliers. This arrangement does not leak at pressures below 20 psig.

The volume of the SIV, which is the enzyme holding and injection unit, is 0.250 ml. For very low concentrations of PFK, the enzyme is first diluted in a reaction solution lacking F6P before being injected into the SIV. During an experiment with purified enzyme, the injected enzymes are always left in the UCSTR with a flow of a nonreactive medium for more than 6 residence times before switching to an input solution containing all reactants.

3.2. Reactor–detector unit

To insure minimal mixing in the connection between the reactor chamber and the sample chamber, the top of the support grid (Fig. 2) is bored out just enough to allow the passage of fluid from the entire ASUM. This space created in this way is enough to trap all gas at the outlet of the reactor chamber during the course of the longest experiments, provided the solutions pumped into the reaction chamber are degassed.

For monitoring downstream from the reactor chamber, a large sampling volume is undesirable: as volume increases, concentration changes in the reactor become increasingly distorted due to the low-pass filter effect of the sample chamber residence time. Therefore, we designed a stirred detection chamber (B, Fig. 1) of volume 0.15 ml, which is negligible compared with the volume of the reaction chamber (1.67 ml). The sampling cell is created by using a flat version of the Orion Ross electrode sealed into the detection chamber by a rubber gasket and a silicone O-ring so that it is precisely positioned to within 1.0 mm of the stirrer shaft when the electrode is screwed down. A copper wire sealed in capillary glass to the shaft of a geared stirrer motor (Edmund Scien-

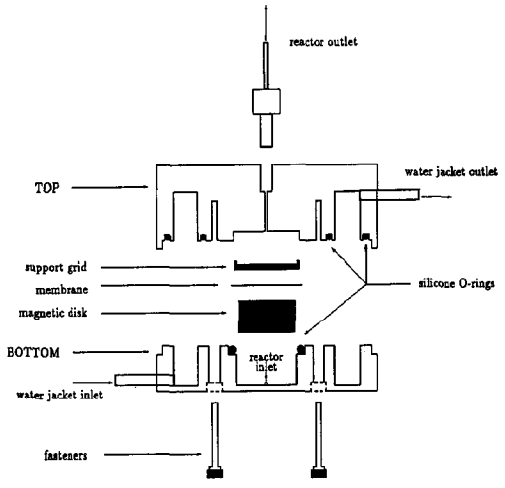

Fig. 2. Cross-section of (A) in Fig. 1: UCSTR reactor in exploded side view. Reactor outer diameter is 3 inch. Diameter of reactor chamber is 0.880 inch; depth of reactor well from bottom of O-ring seating is 0.325 in. A 0.030 inch deep well is cut into top surface of membrane support grid. Other dimensions: membrane support grid diameter is 0.888 in, magnetic stirrer is 0.842 in in diameter and 0.316 in in height, water jacket silicone(S-0604) O-rings are sizes 2–031,2–038 (Parker Seals), reactor O-ring is size 2-119. Four fasteners are threaded into metal inserts in the reactor top to seal the reactor by compression. The reactor's inlet holes (size No. 56), through which 1/16 inch outer diameter tubing is forced and cut off flush to the bottom of the inner reactor wall, were drilled through both the outer and inner walls. The reactor outlet connector is an Upchurch Scientific flangeless fitting for 1/16 inch tubing (1/4–28 thread). Measured volume of reactor chamber once the UCSTR is fully assembled is 1.67 ml.

tific C36,419) that comes up through the bottom of the cell via an O-ring and guide rod assembly allows stirring at any angle. The stirring speed is 74 rpm when the stirrer is supplied with 3 V. Capacitance filtering across the inputs and earth grounding to one end of the supply are necessary to prevent interference with the electrode signal. The detection cell is positioned just above the UCSTR at a 45° angle (Fig. 1). The inlet is narrowed and the outlet enlarged to help bubbles escape. The reference junction is positioned near the inlet, further reducing interference from any possible bubbles that might pass through the system.

3.3. Flow rate monitor

Flow rate is determined with a drop counter, which uses a photocell to detect a drop falling from a tube. A photodiode emits near-infrared light ($\approx$ 900 nm), which is scattered by the drop. The decrease in intensity, as the drop crosses the beam of light, causes a loss of current through the transistor at the detector, which causes the voltage to rise from ground potential. By positioning the emitter and detector farther apart than in the original infrared slotted switch (GE H21A1), and adjusting the threshold at which the voltage rise is considered a drop and not noise, drop monitoring can be made reliable. For the design employed in the UCSTR (a Teflon tube of 1/32 inch inner diameter) drops are well-behaved when the interval between drops is longer than 2 s. The detector must be carefully leveled, because the drop free-falls 1.5 cm to the detector beam. To prevent false readings due to drop oscillation, the detector circuit contains a latch that makes the detector unresponsive for about 60 ms after a drop event. The circuit design is described elsewhere [13].

3.4. Testing and performance calibration

A series of initial experiments was performed in prototype reactors to test for leakage through the ASUM (inability to retain glycolytic enzymes) and for inadequate flushing by the stirrer (inability to keep protein in solution). Leakage proved insignificant when the appropriate membrane was chosen. The quality of flushing was less easy to define, but was deemed acceptable based on two criteria: (1) Tests of protein concentration from the bulk solution of the reactor chamber and from the rinses of the membrane after a trial run at the highest flow rates. (2) Bromothymol blue (BTB) stain of the membrane after a trial run at the highest flow rates. Typically, 98% of the total protein recovered after a trial run of 1 h was found associated with the bulk solution. After 6 h, 85% of the total protein was associated with the bulk solution. Some uncertainty remains in how much protein is truly associated with the

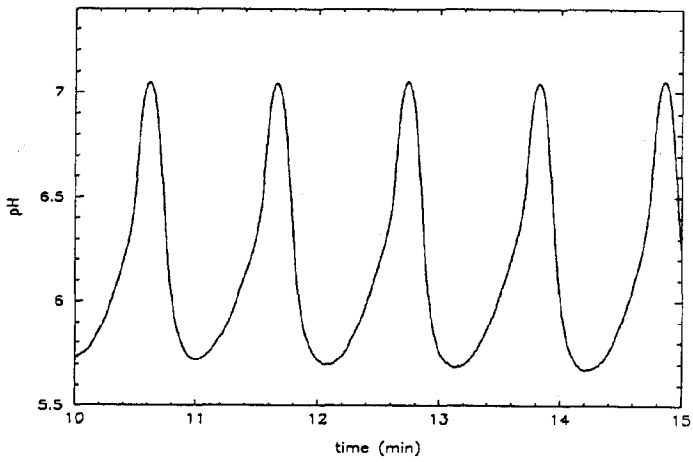

Fig. 3. $Fe(CN)_6^{4-}$–H_2O_2 reaction in a double chamber UCSTR with only top stirrer moving (800 rpm). Flow rate 1.7 ml/min. Bottom chamber assumed to act as a large premixing chamber. YM30 membrane. $[Fe(CN)_6^{4-}]_0 = 3.33$ mM, $[H_2O_2]_0 = 0.10$ M, $[H_2SO_4]_0 = 2.00$ mM, temperature = 25.0 ± 0.1°C.

membrane, due to the lower concentrations found in successive or later rinses and the imperfect recovery of bulk solution from the reactor. The test with BTB showed no color after rinsing the membrane with water. Therefore, little protein was strongly adsorbed. To minimize further adhesion of purified enzyme to the membrane, addition of BSA ensured that the majority of the protein in contact with the membrane was inert.

To examine the effectiveness of stirring and to calibrate the UCSTR's performance, a prototype reactor using combined reaction and detection cells was tested with a known inorganic chemical oscillator, the oxidation of hexacyanoferrate(II)

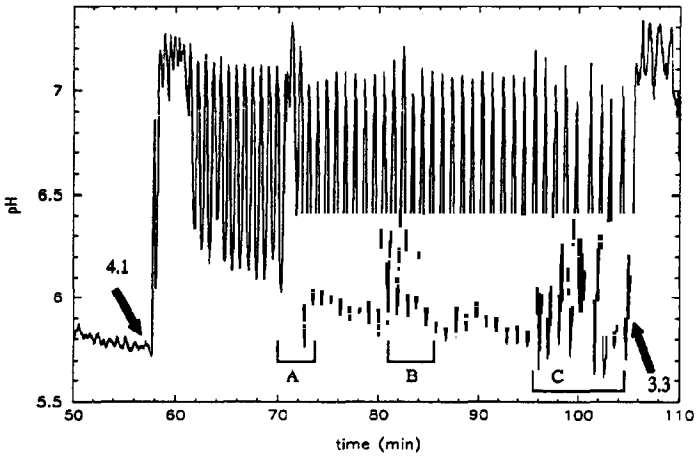

Fig. 4. $Fe(CN)_6^{4-}$–H_2O_2 reaction in a double chamber UCSTR with both stirrers moving. Conditions are the same as in the previous figure except for the variation in stirring. A, B, and C are regions of inadequate stirring due to interference between the magnetic stirrers that caused them to spin at a slower speed. Stirrer settings of 4.1 (≈ 350 rpm) and 3.3 (≈ 250 rpm).

by hydrogen peroxide in unbuffered medium [14]. The two input solutions were prepared [15] with sufficient Triton surfactant (1 ppm in the H_2O_2 input solution) to prevent the formation of gas bubbles in the reactor. Oscillations similar to those previously reported in a different geometry were found (Fig. 3).

Not surprisingly, since the ASUM is unable to block the flow of small ions, oscillations are unaffected by the motion of the bottom stirrer. The prototype's double-chamber reactor acts as one CSTR with a large premixing chamber. When both stirrers are moving at frequencies > 250 rpm, oscillations in both UCSTR and detection chambers are the same (Fig. 4, regions between A and B and between B and C). Variation of stirring speed (Fig. 4) showed that as long as the stirrers moved together at the same frequency, the stirring was adequate. Region A (Fig. 4) shows the effect of momentary stirrer interference before re-entraining and speeding up again. In region B (Fig. 4), the bottom stirrer goes into periodic spurts. In region C (Fig. 4), both stirrers become erratic. Slowing the stirrers to allow them to re-entrain causes degradation of effective mixing and a qualitative change in the behavior of the system. Since the bottom chamber of the final reactor design (Fig. 2) and the prototype are identical, these tests demonstrate the effectiveness of stirring in our UCSTR design.

4. Results

4.1. PFK experiments

Kinetics studies of reaction R1 were carried out to guide studies on the more complex glycolytic system. To determine whether an adequate pH response could be obtained in a buffered medium, reaction R1 was studied in a 30 ml thermostatted closed (batch) reactor using a standard calomel-glass electrode for pH detection. Experiments were performed at low ($\approx 10^{-2}$ M) and high ($\approx 10^{-1}$ M) ionic strength. These experiments demonstrate that a significant response (Fig. 5) can be recorded in the presence of 2 mM buffer. Thus, the initial pH in the experiment is known, and indeed controlled, which is important, since the catalytic activity of PFK is pH sensitive.

In a second experiment, reaction R1 was studied in the double-chamber prototype UCSTR to determine the pH response to a change in flow rate. As the flow rate is decreased 25%, the pH drops from one steady state of the system to

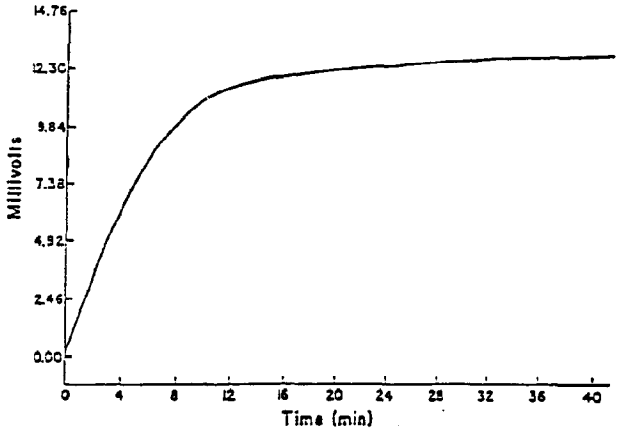

Fig. 5. The pH electrode response versus time for the batch reaction $F6P^{2-} + MgATP^{2-}$ {PFK} → $F1,6DP^{4-} + MgADP^{-} + H^{+}$. Recording is started 12 s after mixing. The pH at time zero on the plot is 6.985: final pH = 6.766, $[ATP]_0 = 0.5$ mM, $[F6P]_0 = 1.0$ mM, [PFK] = 0.1 U/ml (pH 7.0), ionic strength = 0.165 M (100 mM KCl, 50 mM NaCl, 5 mM $MgCl_2$), 2 mM Bis-Tris buffer, pH before mixing = 7.00, temperature = 25.0 ± 0.1°C.

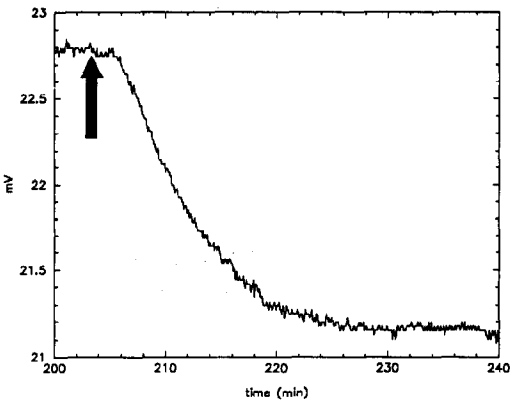

Fig. 6. The pH electrode response versus time for the reaction $F6P^{2-} + MgATP^{2-}$ (PFK) → $F1,6DP^{4-} + MgADP^{-} + H^{+}$ in the UCSTR. Injection of 0.5 U of PFK occurred at time zero. Conditions: $[ATP]_0 = 1.5$ mM, $[F6P]_0 = 1.85$ mM, [PFK] = 0.3 U/ml (pH 8.0), [BSA] = 0.58 mg/ml, salt ionic strength = 0.165 M, 1 mM Bis-Tris buffer, 1 mM phosphate buffer, pH before mixing = 7.30. Arrow: flow rate is changed from 8 ml/h to 6 ml/h, data acquisition rate is 12 min^{-1}. Initial pH = 7.078, final pH = 7.053, temperature = 25.0 ± 0.1°C.

another (Fig. 6). Clearly, the experimental design is capable of detecting very small changes in pH in a reliable manner.

4.2. Muscle extract experiments

Experiments were carried out in the final design UCSTR (Figs. 1 and 2), under conditions for which glycolytic oscillation of metabolites such as ATP and FDP has been reported in batch [16]. Glucose solution was pumped in and the reaction started by injecting the extract with hexokinase in sufficient concentration to give an activity of 0.4 U ml^{-1}. Damped oscillations were found (Fig. 7). Reaction continued for about 4 h after the oscillations stopped (Fig. 7). Decreasing the flow rate by half caused the pH to drop to a value about the same as the maximum of the oscillations in Fig. 8. Doubling the flow rate brought the steady state pH above 6.83, near the initial pH. With these encouraging results, the experiments were refocused on PFK by replacing the added hexokinase and glucose with an input feed of F6P.

With F6P solution as input (Fig. 8), there appear to be high and low pH states above and below pH 6.9, in which PFK is postulated to be "off" and "on", respectively. An initial small oscillation of the same time scale as that seen in Fig. 8

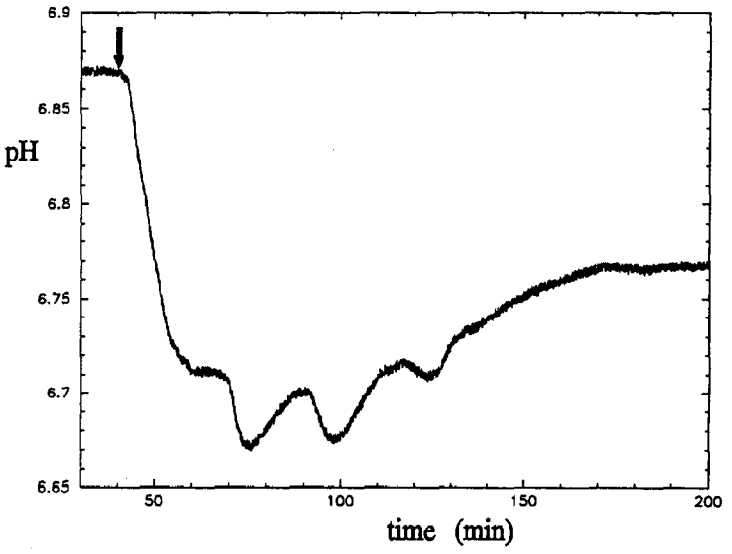

Fig. 7. Glycolytic pH oscillation in UCSTR with 0.4 U/ml hexokinase: $k_0 = 1.77 \times 10^{-3}$ s^{-1}, $[glucose]_0 = 10$ mM, $[ATP]_0 = 1$ mM, $[NAD^{+}]_0 = 10$ μM, [KCl] = 47 mM, [phosphate] = 7.5 mM, [(K^{+})aspartate] = 4 mM, $[MgCl_2] = 8.33$ mM, temperature = 25.0 ± 0.1°C. Arrow: HK and rat skeletal muscle extract (1.2 mg/ml) are injected.

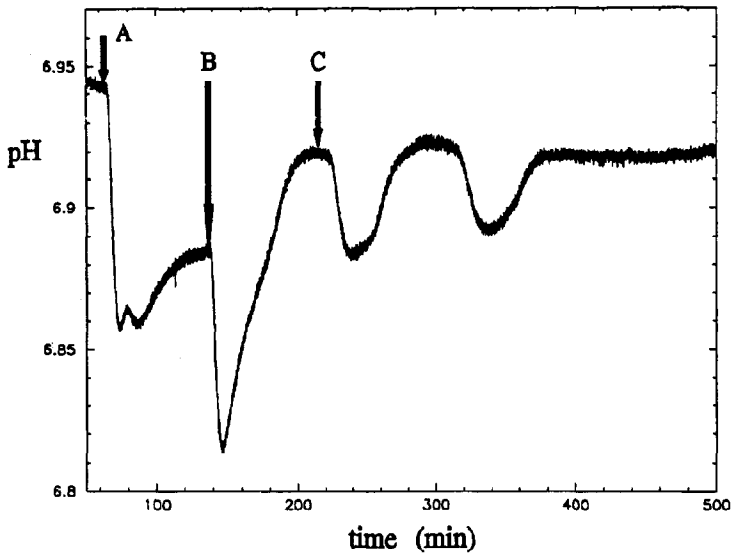

Fig. 8. Glycolytic pH oscillation in the UCSTR: $[F6P]_0 = 0.4$ mM, $[ATP]_0 = 1$ mM, $[NAD^+] = 5$ μM, $[K_2HPO_4] = 7.5$ mM, $[KCl] = 47.0$ mM, $[MgSO_4] = 8.3$ mM, [EDTA] = 1 mM, [dithiothreitol] = 0.18 mM, $[Li_2GTP] = 0.3$ mM, $[(K^+)$aspartate] = 4 mM, pH = 6.951, temperature = 25.0 ± 0.1°C. (A) rat skeletal muscle extract is injected into the UCSTR at steady pH, $k_0 = 1.73 \times 10^{-3}$ s^{-1}, 0.65 mg/ml; (B) additional extract injected, 1.3 mg/ml; (C) $k_0 = 1.51 \times 10^{-3}$ s^{-1}.

is observed between times A and B. After more than an hour (> 7 residence times), the system reaches a low pH steady state. Increasing the extract concentration causes the pH to drop initially, but then the system proceeds to increase in pH toward the high pH steady state above pH

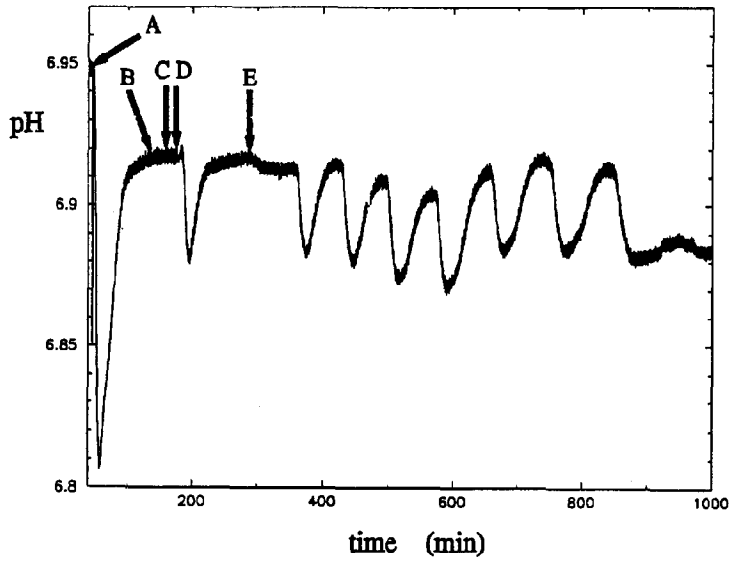

Fig. 9. Glycolytic pH oscillations in the UCSTR. Conditions identical to Fig. 8 except for the following: $[NAD^+] = 1.2$ μM, $pH_0 = 6.955$, $[CaCl_2] = 1.0$ μM. The initial residence time (A) is 9.5 min and the protein concentration in the reactor is 1.2 mg/ml. The flow rate is lowered at (B–E) giving residence times of 10.44, 11.13, 12.85, and 18.50 min, respectively.

6.9. A decrease in the flow rate at time C causes the system to oscillate between the low and high pH states.

A transition from the stable high pH steady state to oscillation was observed upon reducing the flow rate (Fig. 9). Though not as noticeable, because of the difference in time scale, there is a change in the slope below pH 6.9 as the pH rises from the initial drop after injection of the extract. This deflection occurred in Fig. 9 between A and B (and in other experiments); it is interpreted as a slowing down [1] as a system close to oscillatory conditions moves past the low pH state. The excursion between D and E (Fig. 9) also indicates that the system is very close to the oscillatory range. Several reductions in flow rate (Fig. 9, B–E) led to a small pH drop at point E. The system then remained stationary for about 50 min before oscillating spontaneously with a period of $\approx$ 70 min. In each cycle, there is a quick spurt of H^+ lasting 10 min, causing the system to drop to the low pH state; then, the system slowly returns to the high pH state over a period lasting three residence times.

There are two possible interpretations of how the oscillating system resets to the high pH state: (1) reinhibition of glycolysis is slow, (2) reinhibition of glycolysis is as rapid as activation. In (2), rapid reinhibition is followed by a period during which the flow dominates, flushing the system and moving the pH back toward the high pH state. There are several observations that support this view. First, the rising waveform resembles an exponential first-order process. Second, the main contribution to lengthening the period of the last three oscillations is the system remaining for a longer period of time in the low pH state before moving towards the upper pH state. This interpretation is consistent with the longer period oscillation in Fig. 8. Those oscillations, of period $\approx$ 100 min, spend a much longer time in the low pH state before rising exponentially to the high pH state. In the first oscillation, the rise clearly lasts for a period three times the residence time of 11 min. The onset of the second burst of H^+ is delayed by a slow decrease in pH lasting 25 min, which is not observed in the previous experiment.

Oscillations in Fig. 9 stop in the low pH state as opposed to the high steady pH state in Fig. 8. This observation suggests that while glycolysis is still actively occurring, something involved in the regulatory control has failed, leaving the reaction "permanently" in the "on" state. Further experiments were conducted, reproducing the oscillations shown in Fig. 9. Variations of flow rate and [ATP] ($\approx$ 0–2 mM) in these experiments show that under most conditions the high pH state is more experimentally reproducible than the low pH state. It is suggested that the greater stability of the high pH state occurs because that state represents a basal throughput rate of glycolysis when PFK is turned "off". Small amplitude oscillations in the low pH state similar to the single final small amplitude oscillation seen at the far right in Fig. 9 can be found after strong perturbations in pH of short duration (1 min) even 25 h after injecting extract into the experiment.

5. Modeling glycolytic oscillations in the UCSTR

5.1. Mechanism

The mechanism used to model the glycolytic sequence studied in the UCSTR is based on an allosteric multi-subunit enzyme [16], and consists of reactions M1–M6 below (where PEP is phosphoenol pyruvate, PYR is pyruvate, *AK* is adenylate kinase, and adenosine-5′-monophosphate is AMP). Enzymes are not shown in reactions M2 and M4, because M2 requires a series of enzymes and serves only as a "bottleneck" in the pathway, and M4 is included only to complete the stoichiometric sequence. Enzymatic reactants have been italicized for clarity, and species such as H_2O and inorganic phosphate have been eliminated for simplicity. A more complex model involving the coupling of two nonlinear allosteric enzyme mechanisms for PFK and PK under semi-batch conditions [17] was unnecessary, because [PEP] remains too low for the proposed nonlinear PK mechanism to manifest itself. Nevertheless, a variation of this model adapted to flow conditions

is useful, and several kinetics parameters have been taken from that study,

$$PFK + F6P + ATP \longrightarrow FDP + ADP + PFK, \quad (M1)$$

$$FDP + ADP \rightleftharpoons PEP + ATP, \quad (M2)$$

$$PK + PEP + ADP \longrightarrow PYR + ATP + PK, \quad (M3)$$

$$PYR \longrightarrow LAC, \quad (M4)$$

$$AK + ATP + AMP \rightleftharpoons 2ADP + AK, \quad (M5)$$

$$ATPase + ATP \longrightarrow ADP + ATPase. \quad (M6)$$

The rate law expression for reaction M1 can be made to fit a Hill equation; however, several simplifying assumptions must be made for it to do so: (1) the maximum velocity, V_{M1}, of PFK is invariant in the presence of effectors. (2) PFK acts as if it is a protein of two equivalent and independent subunits, each bearing a single site for the allosteric ligands. (3) Each subunit can exist in two conformational states, R (active) and T (inactive) [18]. (4) Equilibrium between the two states is a function of the inhibitor (ATP) and activator (AMP) concentrations. (5) PFK catalysis is "fully concerted", i.e. PFK can exist in only two forms, R (two active subunits) and T (two inactive subunits). To keep the kinetics equations as simple as possible, two further assumptions have been made: extreme cooperativity occurs when all effectors bind in a single step and substrate binds exclusively to the active form of the enzyme.

Table 1
Parameters used in numerical integration of Eqs. (1)–(7)

Parameter	Value
V_{M1} (mM min^{-1})	1.250
V_{M3} (mM min^{-1})	10.000
K_I (mM^2)	0.0016
κ_1	0.173611
K_{M3} (mM)	0.6
k_0 (min^{-1})	0.054
k_2 (mM min^{-1})	0.58
k_{-2} (mM min^{-1})	0.001
k_4 (min^{-1})	0.1
k_5 (min^{-1})	100.0
k_6 (min^{-1})	0.01
$[ATP]_0$ (mM)	1.0
$[F6P]_0$ (mM)	0.4

Table 2
Metal and ligand equilibria used in calculations

Equilibrium reaction	pK_d [a]
$F6P^{2-} + H^+ \rightleftharpoons HF6P^-$	5.8
$F6P^{2-} + Mg^{2+} \rightleftharpoons MgF6P$	1.59
$FDP^{4-} + H^+ \rightleftharpoons HFDP^{3-}$	6.66
$HFDP^{3-} + H^+ \rightleftharpoons H_2FDP^{2-}$	5.86
$FDP^{4-} + Mg^{2+} \rightleftharpoons MgFDP^{2-}$	2.70
$MgFDP^{2-} + H^+ \rightleftharpoons MgFDPH^-$	6.08
$ATP^{4-} + H^+ \rightleftharpoons HATP^{3-}$	6.51
$HATP^{3-} + H^+ \rightleftharpoons H_2ATP^{2-}$	4.06
$ATP^{4-} + Mg^{2+} \rightleftharpoons MgATP^{2-}$	4.06
$MgATP^{2-} + H^+ \rightleftharpoons MgATPH^-$	4.55
$ATP^{4-} + Na^+ \rightleftharpoons NaATP^{3-}$	1.1 [b]
$ADP^{3-} + H^+ \rightleftharpoons HADP^{2-}$	6.40
$HADP^{2-} + H^+ \rightleftharpoons H_2ADP^-$	3.96
$ADP^{3-} + Mg^{2+} \rightleftharpoons MgADP^-$	3.17
$MgADP^- + H^+ \rightleftharpoons MgADPH$	4.91
$ADP^{3-} + Na^+ \rightleftharpoons NaADP^{2-}$	0.8
$HPO_4^{2-} + H^+ \rightleftharpoons H_2PO_4^-$	7.20
Bis-Tris$^- + H^+ \rightleftharpoons$ HBis-Tris	6.50

[a] The pK_d values are for the reverse reaction.
[b] Dissociation constant is assumed to be the same when Na^+ is replaced by K^+.

It will now be useful to define certain parameters and equations. Let the Michaelis–Menten binding constant for F6P in reaction M1 be K_{M1}, and $(K_{M1})^2 = K_1$; and let κ_1 be the ratio of the dissociation constant for the activator bound to the R conformation to the dissociation constant of the inhibitor bound to the T conformation, $\kappa = (K_R^A/K_I^I)^2$. The following velocity equations are defined; k_i refers to a rate constant in reaction (Mi).

$$v_1 = \frac{V_{M1}[F6P]^2}{\left(K_1 + K_1\kappa_1\dfrac{[ATP]^2}{[AMP]^2} + [F6P]^2\right)},$$

$$v_2 = k_2[FDP][ADP] - k_{-2}[PEP][ATP],$$

$$v_3 = \frac{V_{M3}[PEP]}{K_{M3} + [PEP]},$$

$$v_5 = k_5\left([AMP][ATP] - [ADP]^2\right).$$

The UCSTR model is then governed by rate equations (1)–(7) below; k_0 (s^{-1}) is the flow time constant.

$$d[F6P]/dt = k_0([F6P]_0 - [F6P]) - v_1, \quad (1)$$

$$d[FDP]/dt = -k_0[FDP] + v_1 - v_2, \quad (2)$$

$$d[PEP]/dt = -k_0[PEP] + 2v_2 - v_3, \quad (3)$$

$$d[PYR]/dt = -k_0[PYR] + v_3 - k_4[PYR], \quad (4)$$

$$d[ATP]/dt = k_0([ATP]_0 - [ATP]) - v_1 + 2v_2 + v_3 - k_6[ATP] - v_5, \quad (5)$$

$$d[ADP]/dt = -k_0[ADP] + v_1 - 2v_2 - v_3 + k_6[ATP] + v_5, \quad (6)$$

$$d[AMP]/dt = -k_0[AMP] - v_5, \quad (7)$$

5.2. Simulation of pH oscillation

The parameters used in the numerical integration [19] of Eqs. (1)–(7) are collected in Table 1. To simulate pH oscillations in flow, the net flux of glycolysis and ATP hydrolysis in the extract is assumed to be one H^+ per F6P introduced into the mechanism. The glycolytically produced H^+ equilibrates rapidly with conjugate acid–base pairs in the reaction solution. The resulting pH was computed at each step of the simulation of the mechanism ((1)–(7)) and plotted against time (Fig. 10). (COMICS [20], an algorithm for obtaining equilibrium concentrations of all species in multi-metal ion–multi-ligand mixtures (Table 2), was used for the computation.) The waveform and period of the simulation closely match experiment. The amplitude may be smaller because the model does not explicitly consider the NAD^+/NADH cycle. The value for the adenylate kinase catalytic rate constant (k_5) is high, because this enzyme is assumed to be in excess. All the reversible reactions between FDP and PEP have been coalesced into a simplistic single step, because breaking the reaction down into a sequence of more realistic single steps does not influence oscillations, but lengthens the calculation time and requires additional parameters.

5.3. pH calculation from relevant equilibria

A further test of the mechanism is an accurate calculation of pH as a function of time, which is possible because the time scale of equilibration of protonated species is much shorter than that of pH change from glycolysis. A pseudo-steady state equilibrium of the free $[H^+]$ is therefore calculated by treating H^+ as a pseudo-metal ion, and computing its concentration with COMICS [20].

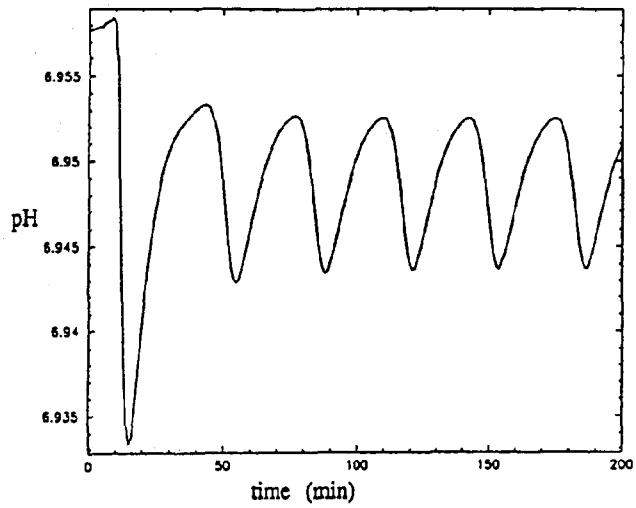

Fig. 10. Glycolytic pH oscillation calculated from model under conditions matching part E in Fig. 9.

Table 3
Summary of calculations using COMICS versus batch experiments. For all runs initial pH = 7.00, [$MgCl_2$] = 5 mM, [PFK] = 0.1 U/ml. Ionic strength = 0.015 M except for last run where it was 0.165 M. Last two runs included 2 mM Bis-Tris

Concentration (mM)		Final pH	
F6P	ATP	calculated	measured
1.00	0.50	6.275	6.31
2.50	1.00	6.342	6.21
2.00	0.50	6.433	6.48
0.50	0.25	6.267	6.30
1.00	0.50	6.700	6.50
1.00	0.50	6.700	6.76

Total [H^+] and ligand concentrations were provided to calculate free [H^+], using the equilibrium quotients gathered in Table 2. To test the accuracy of this type of calculation, a set of batch and flow experiments were performed and the final pH was compared to that expected from a COMICS calculation. A summary of batch experiments at high ionic strength is given in Table 3. In obtaining the experimental data shown in Table 3, the chart recorder was set to pH 7.00 and observed for at least 2 min to verify solution stability. Reaction is initiated by pipetting the appropriate amount of ATP stock solution to bring the total volume to 30 ml quickly. The flow experiments are summarized in Table 4. Two experimental pH values are given: the first is the minimum reached by the initial drop in pH after injecting the enzyme (pH 7.5, volume 0.15 ml), the second is the final steady state pH value. The results are quite good: the worst discrepancy being 0.13 pH unit in batch and 0.3 pH unit in flow.

Table 4
Summary of calculations using COMICS versus flow experiments. For all runs [Na_2F6P] = 0.5 mM, [Na_2ATP] = 3.0 mM, [$MgCl_2$] = 6 mM, [EDTA] = 1 mM, [PFK] = 30 U/ml, [BSA] = 0.5 mg/ml, ionic strength = 0.165 M. (50 mM NaCl, 100 mM KCl), 0.15 mM DTT. First two runs were with 1 mM Bis-Tris. Last two runs were with 1 mM K_2HPO_4. Temperature was 25°C

Calculated [a]		Experiment	
initial pH	final pH	initial pH	final pH
7.357	6.725	7.36	6.83
7.364	6.727	(2.5) [b]	6.98
7.947	6.834	7.95	6.97
7.952	6.834	(2.3) [b]	7.12
7.800	7.072	7.79	6.96
7.788	7.066	(1.9) [b]	7.06
7.264	6.754	7.264	6.813
		(2.1) [b]	6.888

[a] In first three runs, two sets of calculations are shown to bracket the experiment.
[b] Residence time given in minutes results from 30 psig using N_2 pump.

6. Discussion

The major problems encountered in a reactor design based on physical entrapment of enzymes are membrane fouling, protein concentration gradients, and impairment of pump performance. Response to these problems has driven our selection of UCSTR components, the most important of which will be discussed.

6.1. ASUM selection

ASUMs come in three forms: flat sheets or discs, hollow fiber cartridges, and spiral membrane cartridges [8]. Hollow fiber cartridges are a preassembled epoxide-sealed bundle of hollow fibers; spiral membrane cartridges are membrane sandwiches with flow-channel spacers between, the whole assembly glued at the ends. ASUM cartridge assemblies, while providing the most desirable protein gradient prevention scheme, are not available in a disassembled state, and are larger in volume than desirable (*e.g.*, 100 ml). Because of the cartridge geometry, definition of residence time is not the same as in a typical CSTR, since solutes and solvent may make more than one circuit of a second, recirculating pump, necessary for cartridge use, before exiting through the ASUM barrier. Therefore, membrane disc geometry was chosen, because it provides a much more compact, simpler setup to define and model, even though protein gradients are more difficult to control.

Membrane types that comply with our molecular weight cutoffs were arranged in order of decreasing hydrophilicity and tested for flow rate and protein adhesion (which leads to protein gradients). The YM-series had the lowest non-

specific protein binding, a reasonably high flow rate, and lasted through ten cycles of use and cleaning. It was used throughout.

In contrast to commercially available stirred cells, an unconventional upside down configuration was chosen for the UCSTR. Normally, in small cells employing a disc ASUM, the membrane is at the bottom of the reactor with the support grid underneath. A constant gas pressure is applied on top of the liquid surface in the cell for the purpose of concentrating the protein of interest. In this conventional configuration, the stirrer, located above the membrane, shears protein away from the surface. Both gravity and flow act in the same direction to concentrate protein near the membrane surface. A low stirring rate is necessary to prevent a vortex from exposing the ASUM surface to air. The "upside down" UCSTR design minimizes polarization, permits high stirring speed, and works well under pressurized conditions, while facilitating reliable pump performance.

6.2. *Pump performance*

In a conventional CSTR, the procedure of calibrating pump speed only at the start of the experiment is valid, because pump parameters do not change appreciably during an experiment. The pump overcomes a small total resistance throughout the flow-rate range of interest. In the UCSTR, however, outflow blockage by the ASUM results in much greater resistance for the pump to overcome, if there is to be a net flow through the reactor. The resistance can vary from experiment to experiment, if there are significant variations in membrane manufacture, for example, and the resistance can vary within an experiment as the degree of membrane fouling increases.

Several different pump technologies were tested during development of the apparatus, and the one with the best performance was selected. A liquid chromatography N_2 pump had several drawbacks, chief among them the fact that the back pressure, not the flow rate, is held constant, resulting in a lack of control due to pressure overshoot and undershoot. In addition, there is the inconvenience of switching solutions, because the entire pump must be disassembled. A motor-driven syringe pump performed well under low load, but failed under long-term experimental conditions. It stalled sometimes at medium flow rates. Peristaltic pumps overcame these limitations; several types were monitored to find the one with the lowest pulsation.

7. Conclusion

Glycolysis and its key enzyme phosphofructokinase play a critical role in the energy metabolism of many cells and tissues. Interestingly, glycolysis has been shown to exhibit oscillatory behavior both in tissue extracts in batch (from muscle, heart and yeast) and in suspensions of intact cells (yeast, ascites cells) [11,21]. Such oscillatory behavior can be advantageous in the maintenance of a high cellular energy state [12,22,23] and has a greater thermodynamic efficiency [17,24]. Recently there has been increasing interest in oscillatory phenomena in biology and biochemistry, in particular in cytosolic Ca^{2+} signaling [25] and its linkage to metabolic (glycolytic) oscillations in some cases [26,27]. Use of the UCSTR, together with computer simulation of the measured dynamical behavior, such as described here for phosphofructokinase and oscillatory glycolysis, is a promising approach to study the underlying basis of such complicated biochemical phenomena.

Acknowledgement

We thank Mr. Richard Hogan for his assistance in the design and construction of the drop detector. This investigation was supported by research grants CHE-9023294 from the National Science Foundation and DK31559 from the National Institutes of Health (KT).

References

[1] P. Gray and S.K. Scott, Chemical oscillations and instabilities (Oxford Science Publications, Oxford, 1990).

[2] B. Hess and A. Boiteux, Hoppe-Seyler's Z. Physiol. Chem. 349 (1968) 1567.
[3] I. Chibata, ed., Immobilized enzymes, (Halsted Press, New York, 1978).
[4] G.G. Guilbault and W. Stokbro, Anal. Chim. Acta 76 (1975) 237.
[5] K. Eschrich, W. Schellenberger and E. Hoffmann, Acta Biol. Med. Germ. 38 (1979) 25.
[6] L.M. Ellerby, C.R. Nishida, F. Nishida, S.A. Yamanaka, B. Dunn, J.S. Valentine and J.I. Zink, Science 255 (1992) 1113.
[7] J.-F. Hervagault and D. Thomas, Eur. J. Biochem. 131 (1983) 183.
[8] Amicon's Technical Group. Laboratory separation: membrane filtration chromatography Reference publication 716 (Amicon Division W.R. Grace and Co., Danvers, MA, 1987).
[9] R.G. Kemp, Methods Enzymol. 42 (1972) 71.
[10] R.H. Ling, F. Marcus and H.A. Lardy, J. Biol. Chem. 240 (1965) 1893.
[11] K. Tornheim and J.M. Lowenstein, J. Biol. Chem. 249 (1974) 3241.
[12] K. Tornheim, J. Biol. Chem. 263 (1988) 2619.
[13] C.G. Hocker, Ph. D. Thesis, Brandeis University (1992).
[14] Gy. Rábai, K. Kustin and I.R. Epstein, J. Am. Chem. Soc. 111 (1989) 8271.
[15] Gy. Rábai, K. Kustin and I.R. Epstein, J. Am. Chem. Soc. 111 (1989) 3870.
[16] J. Monod, J. Wyman and J.P. Changeux, J. Mol. Biol. 12 (1965) 88.
[17] Y. Termonia and J. Ross, Proc. Natl. Acad. Sci. USA 78 (1981) 2952.
[18] M.R. Waser, L. Garfinkel, M.C. Kohn and D. Garfinkel, J. Theoret. Biol. 103 (1983) 295.
[19] A.C. Hindmarsh, GEAR: Ordinary Differential Equations Systems Solver, Report UCID-3001 (Technical Report, Lawrence Livermore Laboratory, Livermore, CA, 1974).
[20] D.D. Perrin and I.G. Sayce, Talanta 14 (1967) 833.
[21] B. Hess and A. Boiteux, Ann. Rev. Biochem. 40 (1971) 237.
[22] V. Andres, B. Schultz and K. Tornheim, J. Biol. Chem. 265 (1990) 21441.
[23] K. Tornheim, V. Andres and V. Schultz, J. Biol. Chem. 266 (1991) 15575.
[24] P.H. Richter and J. Ross, Biophys. Chem. 12 (1980) 285.
[25] M.J. Berridge and A. Galione, FASEB J. 2 (1988) 3074.
[26] B.E. Corkey, K. Tornheim, J.T. Deeney, M.C. Glennon, J.C. Parker, F.M. Matschinsky, N.B. Ruderman and M. Prentki, J. Biol. Chem. 263 (1988) 4254.
[27] E.A. Longo, K. Tornheim, J.T. Deeney, B.A. Varnum, D. Tillotson, M. Prentki and B.E. Corkey, J. Biol. Chem. 266 (1991) 9314.